Deducing the ^{237}U(n, f) cross section using the surrogate ratio method

J. T. Harke,* L. A. Bernstein, J. Escher, L. Ahle, J. A. Church, F. S. Dietrich, K. J. Moody, and E. B. Norman

Lawrence Livermore National Laboratory, Livermore, California 94551, USA

L. Phair, P. Fallon, R. M. Clark, M. A. Deleplanque, M. Descovich, M. Cromaz, I. Y. Lee, A. O. Macchiavelli,
M. A. McMahan, L. G. Moretto, E. Rodriguez-Vieitez, and F. S. Stephens

Lawrence Berkeley National Laboratory, Berkeley, California 94720, USA

H. Ai and C. Plettner

Yale University, New Haven, Connecticut 06520, USA

C. Beausang and B. Crider

University of Richmond, Richmond, Virginia 23173, USA

We have deduced the cross section for ^{237}U(n, f) over an equivalent neutron energy range from 0 to 20 MeV using the surrogate ratio method. A 55 MeV ^{4}He beam from the 88 inch cyclotron at Lawrence Berkeley National Laboratory was used to induce fission in the following reactions: ^{238}U($\alpha, \alpha' f$) and ^{236}U($\alpha, \alpha' f$). The ^{238}U reaction was a surrogate for ^{237}U(n, f), and the ^{236}U reaction was used as a surrogate for ^{235}U(n, f). Scattered α particles were detected in a fully depleted segmented silicon telescope array over an angle range of $35°$ to $60°$ with respect to the beam axis. The fission fragments were detected in a third independent silicon detector located at backward angles between $106°$ and $131°$.

PACS number(s): 24.50.+g, 24.75.+i

I. INTRODUCTION

Neutron-induced fission cross sections are of interest for a variety of applied and basic science reasons. To further our understanding of fission, we employed the surrogate ratio method described by Plettner *et al*. [1,2] to determine the ^{237}U(n, f) cross section via comparison with the well-measured ^{235}U(n, f) cross section. This technique removes and/or reduces a large number of systematic and theoretical uncertainties related to the direct surrogate method [3,4]. In this report, we review the surrogate ratio method as it pertains to fission, describe the experiment, and present the resulting ^{237}U(n, f) deduced cross section.

II. THE SURROGATE RATIO METHOD

The surrogate ratio method or, simply, the ratio method is an indirect technique that allows the determination of cross sections for compound-nucleus reactions involving difficult-to-produce targets. The method is a variant of the so-called surrogate nuclear reaction approach in that it uses a light-ion-induced reaction to determine the decay probability of the same compound nucleus (CN) that occurs in the desired difficult-to-measure reaction. However, the ratio method requires that the decay probabilities of two similar CN are measured relative to one another. The second CN has to occur in a reaction that is similar to the difficult-to-measure desired reaction and for which the cross section is known. In this report, we

use the known ^{235}U(n, f) cross section to obtain the cross section for ^{237}U(n, f) for neutron energies up to 20 MeV. The following reviews the surrogate nuclear reaction idea, explains the motivation for considering simplifications of the approach, and outlines the ratio method.

The surrogate nuclear reaction technique is an indirect method to determine the cross section for a particular type of "desired" reaction, $a + A \rightarrow B^* \rightarrow c + C$, that proceeds through a CN state B^*, which is a highly excited state in statistical equilibrium [5–14]. The formation and decay of a CN with a given angular momentum and parity are independent of each other. In such situations, the cross section for the desired reaction can be (somewhat schematically) expressed as

$$\sigma_{\alpha\chi}(E_a) = \sum_{J,\pi} \sigma_\alpha^{CN}(E_{ex}, J, \pi) \; G_\chi^{CN}(E_{ex}, J, \pi) \,. \quad (1)$$

Here α denotes the entrance channel $a + A$ and χ represents the relevant exit channel $c + C$. E_a is the kinetic energy of the projectile a, and E_{ex} is the excitation energy of the compound nucleus B^*; they are related via the separation energy S_a of the projectile in the nucleus B: $E_{ex} = S_a + E_a$. In this present work, we are interested in the reactions $n + {}^{235}$U $\rightarrow$ ^{236}U$^* \rightarrow$ fission and $n + {}^{237}$U $\rightarrow {}^{238}$U$^* \rightarrow$ fission. In many cases the formation cross section $\sigma_\alpha^{CN} = \sigma(a + A \rightarrow B^*)$ can be calculated adequately by using optical potentials, while the theoretical decay probabilities G_χ^{CN} for the different channels χ are often quite uncertain. The objective of the surrogate method is to experimentally determine or constrain these decay probabilities.

―――――
*Electronic address: harke2@llnl.gov

In a surrogate experiment, the compound nucleus B^* is produced via an alternative (surrogate) direct reaction $d + D \rightarrow b + B^*$, and the decay of B^* is observed in coincidence with the outgoing particle b. In the experiment, the relevant compound nuclei $^{236}U^*$ and $^{238}U^*$ were produced via inelastic α scattering, $^{236,238}U(\alpha, \alpha')$. Fission fragments were detected in coincidence with scattered α particles. The probability for forming B^* in the surrogate reaction (with specific values for the excitation energy E_{ex}, angular momentum J, and parity π) is $F_\delta^{CN}(E_{ex}, J, \pi)$, where δ refers to the entrance channel $d + D$. The quantity

$$P_{\delta\chi}(E_{ex}) = \sum_{J,\pi} F_\delta^{CN}(E_{ex}, J, \pi) \; G_\chi^{CN}(E_{ex}, J, \pi) , \quad (2)$$

which gives the probability that the compound nucleus B^* was formed with energy E_{ex} and decayed into channel χ, can in principle be obtained experimentally.

The direct-reaction probabilities $F_\delta^{CN}(E_{ex}, J, \pi)$ have to be determined theoretically so that the branching ratios $G_\chi^{CN}(E_{ex}, J, \pi)$ can be extracted from the measurements. In practice, the decay of the compound nucleus is modeled using statistical reaction theory, and the $G_\chi^{CN}(E_{ex}, J, \pi)$ are obtained by adjusting parameters in the calculations to reproduce the measured decay probabilities $P_{\delta\chi}(E_{ex})$. Subsequently, the branching ratios obtained in this manner are inserted into Eq. (1) to yield the desired reaction cross section.

The experimental determination of the decay probability $P_{\delta\chi}(E_{ex}) = N_{\delta\chi}/N_\delta$ requires that both the number of b-χ coincidences $N_{\delta\chi}$ and the number of reaction events N_δ (the total number of inelastically scattered α particles in the present case) are accurately determined. If target contaminants are present, it becomes very difficult, if not impossible, to determine a reliable value for N_δ.

The surrogate ratio method eliminates the need to accurately measure N_δ, the total number of reaction events, which has been the source of the largest uncertainty in surrogate experiments performed recently [1,3]. Under the proper circumstances, it also reduces or removes dependence on the angular distribution of fission fragments, which is not well characterized in the present experiments. The goal of the ratio method is to experimentally determine the ratio

$$R(E) = \frac{\sigma_{\alpha_1\chi_1}(E)}{\sigma_{\alpha_2\chi_2}(E)} \quad (3)$$

of the cross sections of two compound-nucleus reactions, $a_1 + A_1 \rightarrow B_1^* \rightarrow c_1 + C_1$ and $a_2 + A_2 \rightarrow B_2^* \rightarrow c_2 + C_2$, for the same excitation energy, $E \equiv E_{ex_1} = E_{ex_2}$ of both compound nuclei. An independent determination of one of the above cross sections then allows one to infer the other by using the ratio $R(E)$.

Under certain conditions [15,16] the branching ratios $G_\chi^{CN}(E_{ex}, J, \pi)$ become independent of J and π; i.e., the Weisskopf-Ewing limit of the statistical Hauser-Feshbach theory applies. The form of the cross section (for the desired reaction) simplifies to $\sigma_{\alpha\chi}^{WE}(E_{ex}) = \sigma_\alpha^{CN}(E_{ex}) \, G_\chi^{CN}(E_{ex})$, where $\sigma_\alpha^{CN}(E_{ex}) = \sum_{J\Pi} \sigma_\alpha^{CN}(E_{ex}, J, \pi)$ is the reaction cross section describing the formation of the compound nucleus at energy E_{ex}, and $G_\chi^{CN}(E_{ex})$ denotes the $J\pi$-independent branching

ratio for the exit channel χ. In the Weisskopf-Ewing limit, the ratio $R(E_{ex})$ can be written as

$$R(E_{ex}) = \frac{\sigma_{\alpha_1}^{CN}(E_{ex}) \, G_{\chi_1}^{CN}(E_{ex})}{\sigma_{\alpha_2}^{CN}(E_{ex}) \, G_{\chi_2}^{CN}(E_{ex})} , \quad (4)$$

with branching ratios G_χ^{CN} that are independent of the $J\pi$ population of the compound nuclei under consideration. For most cases of interest, the compound-nucleus formation cross sections $\sigma_{\alpha_1}^{CN}$ and $\sigma_{\alpha_2}^{CN}$ can be calculated using an optical model. To determine $G_{\chi_1}^{CN}/G_{\chi_2}^{CN}$, two experiments are carried out. Both use the same direct-reaction mechanism $D(d, b)B^*$, but different targets D_1 and D_2, to create the relevant compound nuclei B_1^* and B_2^*, respectively. For each experiment, the number of coincidence events, $N_{\delta_1\chi_1}^{(1)}$ and $N_{\delta_2\chi_2}^{(2)}$, are measured.

In the present case, $^{236}U(\alpha, \alpha') \, ^{236}U^*$ and $^{238}U(\alpha, \alpha') \, ^{238}U^*$ experiments were carried out, and α-fission coincidences were measured. The same experimental setup was employed for both cases. The ratio of the branching ratios into the desired channel for the compound nuclei created in the two reactions is given by

$$\frac{G_{\chi_1}^{CN}(E_{ex})}{G_{\chi_2}^{CN}(E_{ex})} = \frac{N_{\delta_1\chi_1}^{(1)}(E_{ex})}{N_{\delta_2\chi_2}^{(2)}(E_{ex})} \times \frac{N_{\delta_2}^{(2)}(E_{ex})}{N_{\delta_1}^{(1)}(E_{ex})}. \quad (5)$$

If both experiments give the same number of reaction events, $N_{\delta_1}^{(1)} \approx N_{\delta_2}^{(2)}$, the ratio of the decay probabilities simply equals the ratio of the coincidence events, and the quantity $R(E_{ex})$ becomes

$$R(E_{ex}) = \frac{\sigma_{\alpha_1}^{CN}(E_{ex}) \, N_{\delta_1\chi_1}^{(1)}(E_{ex})}{\sigma_{\alpha_2}^{CN}(E_{ex}) \, N_{\delta_2\chi_2}^{(2)}(E_{ex})}. \quad (6)$$

In taking the ratio of identical reactions on different target nuclei, we have removed our dependence on the Hauser-Feshbach theory. In practice, it is unlikely that both experiments yield the same number of reaction events, and it becomes necessary to apply a correction to account for the difference in target thickness, integrated beam on target, and live time of the data acquisition for the two experiments.

III. EXPERIMENTAL APPARATUS

The present experiment was performed at the 88 inch cyclotron at Lawrence Berkeley National Laboratory using the silicon telescope array for reactions studies (STARS) developed by Lawrence Livermore National Laboratory. Inelastically scattered α particles from the $^{238}U(\alpha, \alpha' f)$ and $^{236}U(\alpha, \alpha' f)$ reactions were detected using the STARS scattering chamber shown schematically in Fig. 1. The silicon telescope produces differential energy loss in the thin (ΔE) and thick (E) detectors, which enables particle identification. The ΔE and E detectors are both Micron S2 type with a thickness of 140 and 1000 μm, respectively. Each S2 detector has 48 rings on one side and 16 sectors on the other. For this experiment both detectors had pairs of adjacent rings and sectors bussed together to form twenty-four 1 mm wide rings and eight sectors. The targets were located 16 mm upstream
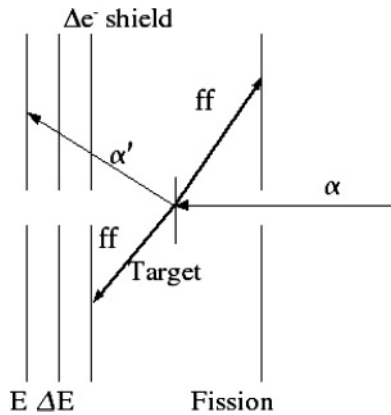
FIG. 1. STARS detector setup with silicon telescope downstream from target and fission detector 10 mm upstream of target. The Δe^- shield located in front of the ΔE detector ranged out the fission fragments.

FIG. 2. Typical ^{226}Ra calibration spectrum for an individual ring. Data show the five dominant α particles present in the ^{226}Ra decay chain vs channel number in the SILENA ADC.

of the front face of the ΔE detector. The ΔE and E detectors were spaced 3 mm apart. The beam spot on the target was approximately 3 mm in diameter. This geometry leads to an angular detection range in θ (the angle formed between the beam axis and the scattered α particle) from 35° to 60°. The trajectory of an α particle was determined by which rings in the ΔE and E detector were triggered. The angular resolution limited the precision of the recoil energy correction applied to the scattered α particle. A 4.44 mg/cm^2 aluminum foil was placed between the target and the silicon telescope. The aluminum foil served a dual purpose. The foil ranged out the fission fragments thereby protecting the ΔE detector from damage which would reduce its energy resolution. The foil was also biased to 300 V during the experiment to help reduce the effect of δ electrons produced in the target. Fission fragments were detected in a third 140 μm Micron S2 detector located 10 mm upstream of the target. The adjacent rings and sectors of this detector were also bussed together. The fission detector covered an angle range of 106° to 131° with respect to the beam axis of the telescope.

The ΔE, E, and fission detectors were biased with 30, 105, and 30 V, respectively. The signals from the rings and sectors of the ΔE and E detectors were conducted through the vacuum chamber wall by four straight-through 34-pin connectors potted into a custom-made NEMA-G10 vacuum flange. The signals were preamplified by 64 individual 45 mV/MeV CHARGE8V Swan Research preamplifiers located on the side of the STARS scattering chamber. The amplified signals were connected to four 16-channel CAEN N568B shapers by 64 individual 10 m long RG-174 cables. The signals from the fission detector were treated identically with the exception that the preamplifiers used had a sensitivity of 8 mV/MeV. The fast output of the CAEN N568B shapers were connected to LeCroy 1806 discriminators modified to be leading edge. The discriminator thresholds were set at 60 mV, which corresponds to an energy threshold of approximately 800 keV. At least one hit in each ΔE and E detector were required to form the particle trigger. Once a valid trigger occurred, the delayed shaped slow output of the shaper channels were digitized by
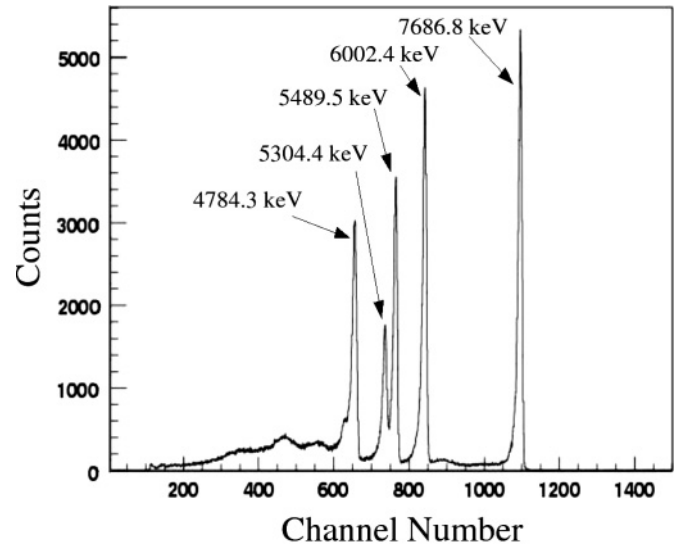
96 channels of SILENA analog-to-digital converters (ADCs). The gate provided to the SILENA ADCs was approximately 7 μs long. Particle-fission timing was obtained using a time-to-amplitude converter (TAC) module readout using an Ortec AD413 peak-sensing ADC.

IV. DETECTOR CALIBRATION

The ΔE and E silicon detectors were calibrated using a ^{226}Ra α source. A typical calibration spectrum is shown in Fig. 2. The peaks were fited with a skewed Gaussian in order to account for the effects of incomplete charge collection in the silicon. Typical values for σ were between 31 and 46 keV for the rings on the ΔE detector and 22 to 30 keV for the rings on the E detector. The sectors of both detectors had a factor of approximately 1.4 poorer energy resolution ($\Delta E/E$). In order to obtain the best energy resolution possible, the rings were used to reconstruct the energy of the α particle events. The 1σ energy resolution of the combined detectors was taken as the sum of the squares of the individual uncertainties and ranged between 38 and 55 keV.

V. OBSERVATIONS

Data were taken over a period of five consecutive days at the 88 inch cyclotron using a 55 MeV beam of α particles with an intensity of 2 to 5 pnA. The ΔE-E overlap coincidence time window was adjusted to be approximately 50 ns. The ^{238}U fission data were obtained from a self-supporting metallic 3619 $\pm$ 72 Å (585 $\pm$ 23 μg/cm^2) thick ^{238}U foil. The ^{236}U fission data were obtained using a uranyl nitrate ^{236}UO$_2$(NO$_3$)$_2$ target consisting of 99.68% ^{236}U and 0.32% ^{234}U electroplated onto a 2.3 mg/cm^2 Ta foil. The ^{236}U foil had an areal density of approximately 184 $\pm$ 9 μg/cm^2. The areal density of
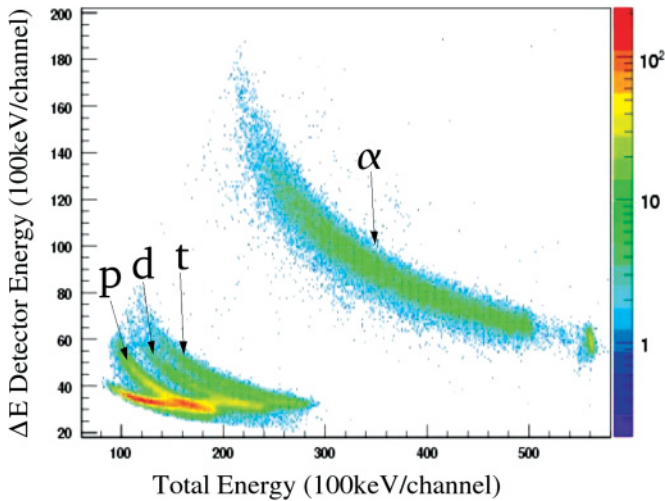
FIG. 3. (Color) ΔE vs $(\Delta E + E)$ plot obtained from nominally 55 MeV α particle incident on ^{238}U in coincidence with fission events. Starting in the lower left corner, we see protons, deuterons, and tritons. The large band in the middle of the plot represents α particles.

FIG. 4. (Color) Effective thickness energy curve. Particles bands are designated as in Fig. 3.

each target was determined by its area and specific activity. The master trigger rate for coincident events ranged between 4 and 6 kHz during the experiment. The data acquisition system event deadtime was set by the master gate width of 70 μs. At master trigger rates of 4 and 6 kHz, the system deadtime was 28% and 42%, respectively. The fission detector singles rate was considerably higher at 40 kHz. This was due to a large (approximately 1 b) ^{238}U(α, f) fusion-fission cross section. The fusion-fission rate produced a random background in the fission spectrum at the level of 10%. This was corrected for by making a prompt particle fission time gate using the particle fission TAC as well as an off-prompt gate. The observed random events were corrected for the difference in time of the two gates and the weighted background was subtracted from the prompt events.

The protons, deuterons, tritons, ^{3}He, and α particles were uniquely identified by plotting ΔE against the total energy $(\Delta E + E)$ to create a particle identification (PID) plot as shown in Fig. 3. The PID plot for each ring was linearized to create an effective thickness vs energy plot, which was generated using the following linearization function, where R is the range, $E_{\rm tot}$ is the total particle energy, and E is the energy deposited in the E detector.

$$R = 15.0\left(E_{\rm tot}^{1.75} - E^{1.75}\right). \tag{7}$$

Figure 4 shows a typical effective thickness energy curve for an individual ring. α particle events were defined as particles that occurred within an energy range of 2σ (approximately 400 keV) of the centroid of the α particle band. This range energy cutoff ensures that the data from the ^{236}U and ^{238}U are free from $(^4$He,^{3}He) induced fission events. Events in the fission detector greater than 6 MeV (approximately channel 200 in Fig. 5) were identified as fission events to remove light ions from direct reactions and charged-particle evaporation. The fission fragments lose considerable energy in the target and detector dead layer before they are detected. A typical
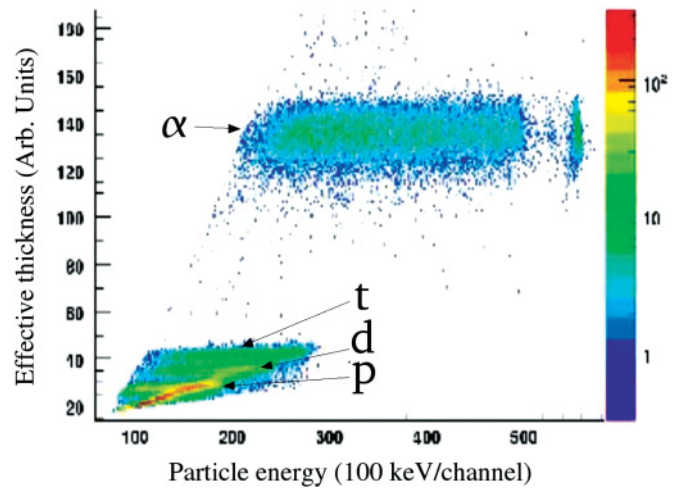
fission spectrum for an individual ring is shown in Fig. 5. The uncertainty in determining the cutoff point at the minimum of the fission spectrum introduces a systematic uncertainty in the final ^{237}U(n, f) cross section. The sensitivity of the final cross section to the fission cutoff point was determined to be 1.3% and is listed in Table I.

For each ring in the ΔE detector, a PID plot and range curve were created. The α particles, identified in the effective thickness energy plot, in coincidence with fission events were identified by the sort routine. A histogram of α-fission coincidences as a function of α-particle energy was created for each ring in the ΔE detector. The energy bins for the histogram were chosen to be 100 keV wide. A bin size of 100 keV was chosen due to the statistics per bin and in order to allow for compression at a later time. The α-particle energy was corrected event by event for recoil effects and for energy losses in the target, aluminum δ shield, and inert detector layers (Al and Au). The spectra for each ring were then summed together. This process was identical for both ^{238}U$(\alpha, \alpha' f)$ and ^{236}U$(\alpha, \alpha' f)$ data. The data were also corrected to take into account the integrated beam current, number of target atoms,
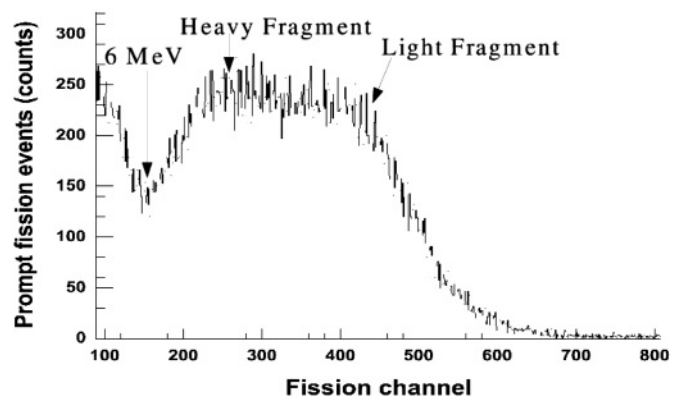

FIG. 5. Typical fission spectrum from a ring in the fission detector. Centroids of the light and heavy fission fragments are indicated with arrows.

TABLE I. Sources of systematic uncertainty for the ^{238}U/^{236}U ratio.

Affected parameter	Source of uncertainty	Relative uncertainty (%)
Normalization factor	^{238}U target thickness	5
Normalization factor	^{236}U target thickness	5
α spectra	Fission spectrum cutoff energy	1.3
Total systematic uncertainty		7.2

TABLE II. Systematic sources of energy uncertainty.

Sources	ΔE (keV)
Energy straggle (δ shield and target)	$38-85$
Recoil angle	$19-54$
Intrinsic detector energy resolution	$38-55$
Cyclotron beam	60
Total uncertainty	$157-220$

and live time of the acquisition system. This normalization factor is

$$\text{Norm} = \frac{I_{^{236}\text{U}}}{I_{^{238}\text{U}}} \times \frac{T_{\text{Live}^{236}\text{U}}}{T_{\text{Live}^{238}\text{U}}} \times \frac{N_{\text{Atoms}^{236}\text{U}}}{N_{\text{Atoms}^{238}\text{U}}} = 0.1534, \quad (8)$$

where $I_{^{23x}\text{U}}$ is the integrated beam current, $T_{\text{Live}^{23x}\text{U}}$ is the live-time fraction, and $N_{\text{Atoms}^{23x}\text{U}}$ are the number of atoms of the corresponding target. The uncertainties associated with the live-time fraction and integrated beam current are less than a percent. The uncertainty in the target thicknesses mentioned above is the dominant uncertainty in the normalization factor and is listed in Table I.

The final α fission spectra are given by

$$N(E_{\text{ex}})_{^{238}\text{U}_{\text{fission}}} = N(E_{\text{ex}})_{^{238}\text{U}_{\alpha\text{-}f}}, \quad (9)$$

and

$$N(E_{\text{ex}})_{^{236}\text{U}_{\text{fission}}} = \frac{N(E_{\text{ex}})_{^{236}\text{U}_{\alpha\text{-}f}}}{\text{Norm}}, \quad (10)$$

where $N(E_{\text{ex}})_{^{23x}\text{U}_{\text{fission}}}$ are the corrected fission spectra, $N(E_{\text{ex}})_{^{23x}U_{\alpha\text{-}f}}$ are the α-fission coincident spectra described above, and Norm is the normalization factor from Eq. (8). Figure 6 shows the resulting spectra corrected for the
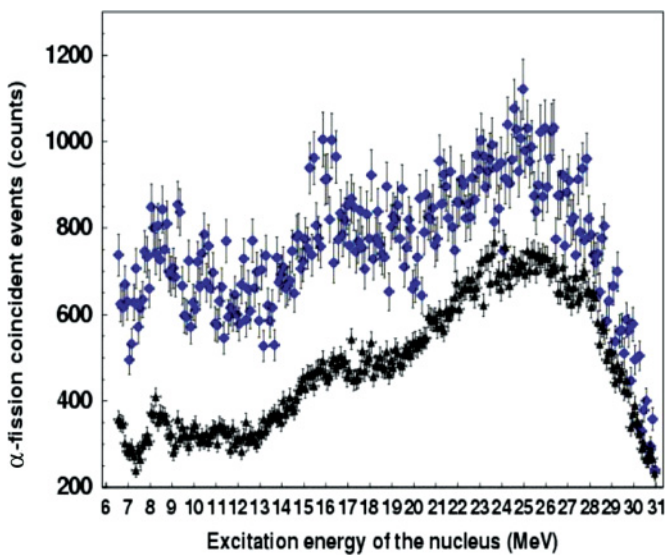
normalization factor. The α-U Coulomb barrier (24 MeV) and the recoil of the target nucleus limit the maximum excitation energy that can be studied to approximately 26 MeV.

VI. SYSTEMATIC UNCERTAINTIES

A detailed analysis of the energy loss and uncertainty in the detector system has been performed. The sources of uncertainty are energy straggle, angular resolution, intrinsic detector energy resolution, and cyclotron beam energy resolution, and they are documented in Table II. The energy straggle arises from the interaction of the α particles with the various materials in the target and detector system. α particles interact with the target material, δ shield, aluminum, and gold layers on the detector, and the silicon. The energy losses in the inactive layers are substantial (700 keV to 2 MeV) and are corrected on an event by event basis in the data analysis. The energy loss corrections take into account the energy of the incident α particle and the angle at which it is incident. Typical values of energy loss are given in Table III. The angular resolution of the detector is dictated by the geometry of the beam spot on the target and the relative distances of the target to the ΔE and E detectors.

For this experiment, the angular resolution ranged between $0.7°$ and $2.2°$. The angular resolution translates into an uncertainty of the recoil angle of the target nucleus. The intrinsic detector resolution was measured using the ^{226}Ra source described in Sec. IV. The cyclotron beam energy resolution was inferred from the width of the elastic peak in a previous experiment. In that experiment, the beam width

FIG. 6. (Color) Number of $(\alpha, \alpha' f)$ events as a function of excitation energy. These data are used to calculate relative probability of fission for these nuclei. ^{238}U (triangles) compared to ^{236}U (circles).

TABLE III. Materials responsible for energy loss.

Detector element	Material	Areal density ($\mu g/\text{cm}^2$)	E_{loss} (keV)
^{238}U target	^{238}U	292	$18-52$
^{236}U target	^{236}U	92	$6-15$
^{181}Ta backing (^{236}U target only)	^{181}Ta	2300	$150-418$
δ shield	Aluminum	4440	$508-1534$
Detector contacts (sectors)	Gold	1158	$73-200$
Detector contacts (rings)	Aluminum	27	$19-33$
Total energy loss for ^{238}U target and detector			$682-1744$
Total energy loss for ^{236}U target and detector			$838-2128$

was measured by placing a calibrated silicon detector directly in the α beam from the 88 inch cyclotron [17]. The energy width of the cyclotron beam was then inferred using the relation

$$\Delta E_{\text{total}}^2 = \Delta E_{\text{cal}}^2 + \Delta E_{\text{beam}}^2, \tag{11}$$

where E_{total} is the total energy uncertainty, E_{cal} is the intrinsic detector resolution, and E_{beam} is the cyclotron beam energy width. The energy uncertainty changes as a function of outgoing α-particle angle; therefore, the energy straggle and recoil angle uncertainty partially cancel each other. As a final check on the energy uncertainty, the elastic peak was fit with a Gaussian and the 1σ uncertainty was found to be 220 keV. Based on this and the above calculations, the overall energy uncertainty used in the final cross section was taken to be 220 keV.

The fission fragments have a distribution with respect to the recoiling nucleus that is anisotropic. This anisotropy changes with the excitation energy of the nucleus. Differences in the anisotropy of the fission fragments [18] with respect to the recoiling ^{236}U and ^{238}U nuclei constitute another source of uncertainty due to the finite solid angle coverage of the fission detector. The fission fragment anisotropies for ^{238}U and ^{236}U fission fragments have been examined as shown in Fig. 7. As a measure of the anisotropy, we consider the ratio of the number of fission events in the angular range of $0°$ to $30°$ to the number of fission events over the angle range of $45°$ to $80°$, as a function of excitation energy. The angle described here is taken with respect to the recoiling uranium nucleus. In the energy range near the fission barrier, from 0 to 4 MeV surrogate neutron energy (6.4 to 10.4 MeV excitation energy), the anisotropy peaked at a factor of 3 and dropped to unity by 4 MeV surrogate neutron energy for both nuclei. The main feature to note is that the ratio of the fission fragment
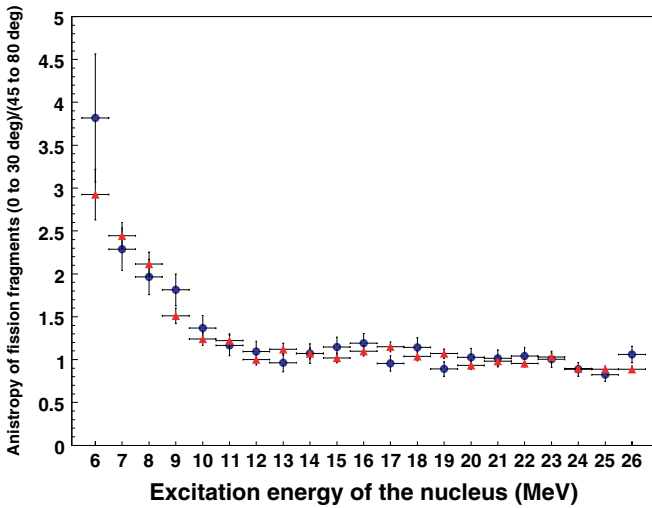

FIG. 7. (Color) In-plane fission fragment anisotropies as a function of excitation energy of the nucleus for ^{238}U (red triangles) and ^{236}U (blue circles). Anisotropy is most pronounced at the fission barrier E_{ex} of approximately 6 MeV and decreases toward unity thereafter. Fission anisotropies are equal within the experimental uncertainties over the excitation energy range of interest.
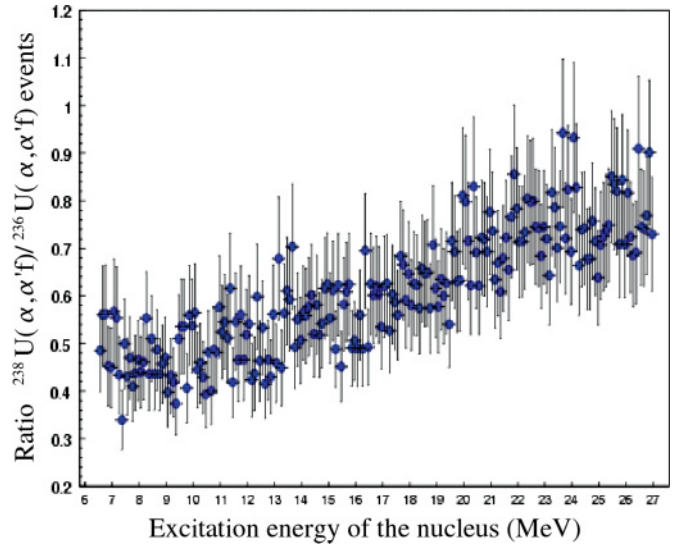

FIG. 8. (Color) Ratio of ^{238}U$(\alpha, \alpha' f)$ to ^{236}U$(\alpha, \alpha' f)$ events as a function of excitation energy of the corresponding nucleus.

anisotropies of ^{238}U over ^{236}U was found to be consistent with unity in the energy range from 0 to 20 MeV surrogate neutron energy (6 to 26 MeV in excitation energy). The ratio method reduces our sensitivity to the fission fragment anisotropies provided the two nuclei have similar distributions as is the case here.

VII. ^{237}U(n, f) CROSS SECTION RESULTS

The ^{237}U(n, f) cross section was determined from the data using the procedure described in Sec. II. The normalized ratio $R(\frac{238}{236}) = N(E_{\text{ex}}, ^{238}U_{\text{fission}})/N(E_{\text{ex}}, ^{236}U_{\text{fission}})$ was determined as a function of excitation energy and is plotted in Fig. 8. The ^{235}U(n, f) cross section energy scale was converted to excitation energy by adding the ^{236}U neutron separation energy ($S_n = 6544.5$ keV). The product of the $R(\frac{238}{236})$ ratio and the ^{235}U(E_{ex}) spectrum yields the ^{237}U(E_{ex}, n, f) spectrum in excitation energy. The final result is obtained by shifting the ^{237}U(E_{ex}, n, f) energy scale down by subtracting the ^{238}U neutron separation energy ($S_n = 6152.0$ MeV) to obtain the ^{237}U(n, f) cross section at the appropriate neutron energy. This procedure is summarized in the following equations.

$$N(^{235}U(E_{\text{ex}}, n, f)) = N(^{235}U(E_n + S_n(^{236}U), n, f)), \tag{12}$$

$$N(^{237}U(E_{\text{ex}}, n, f)) = \frac{N[^{238}U(E_{\text{ex}}, (\alpha, \alpha' f))]}{N[^{236}U(E_{\text{ex}}, (\alpha, \alpha' f))]},$$
$$\times N(^{235}U(E_{\text{ex}}, n, f)) \tag{13}$$

$$N(^{237}U(E_n, n, f)) = N(^{237}U(E_{\text{ex}} - S_n(^{238}U), n, f)). \tag{14}$$

The upper panel of figure 9 shows the the ^{235}U(n, f) cross section [19] used to obtain the ^{237}U(n, f) cross section. The resulting ^{237}U(n, f) cross section is plotted in the lower panel of Fig. 9. For completeness, previous results from Younes and Britt [20] are also shown. The two cross sections agree well in the neutron energy range from 0 to about 10 MeV. Above 10 MeV, our cross section is lower by 10−20%. This difference
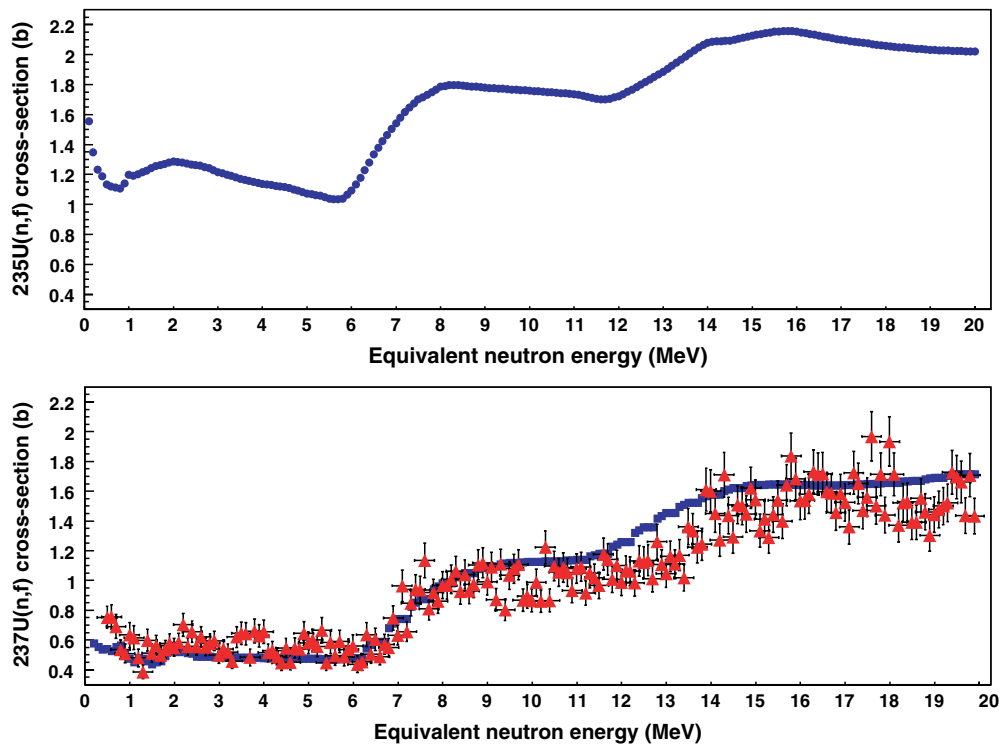
FIG. 9. (Color) Upper panel shows ^{235}U(n, f) cross section from ENDF/B-VII [19] used to determine ^{237}U(n, f) cross section. Lower panel compares our ^{237}U(n, f) cross section (red triangles) to results from earlier work by Younes and Britt [20] (blue squares, no error bars).

may arise from the linear extrapolation to higher energies of first and second chance fission used by Younes and Britt.

VIII. CONCLUSIONS

The ^{237}U(n, f) cross section has been determined using the surrogate ratio method. This method requires that a fission cross section for a similar nucleus be known. In this experiment, the reaction ^{238}U$(\alpha, \alpha' f)$ was used as a surrogate reaction for ^{237}U(n, f) and the reaction ^{236}U$(\alpha, \alpha' f)$ as a surrogate reaction for the known case of ^{235}U(n, f). In using the surrogate ratio method, the assumption was made that the inelastic (α, α') scattering cross sections for the two nuclei (^{238}U and ^{236}U) are equal to within approximately 5%. We also assumed that the compound nucleus formations at equivalent neutron energies in the range $0-20$ MeV are equal to within approximately 5%. These two assumptions lead to an uncertainty in the ^{237}U(n, f) cross section of no greater than 10% over the energy range $0-20$ MeV equivalent neutron energy. The surrogate ratio method minimizes uncertainties

arising from preequilibrium decay, angular momentum effects, and fission fragment anisotropies. These adverse effects impact both reactions considered here in a similar manner, and their effects are expected to approximately cancel in the ratio method.

[1] C. Plettner *et al.*, Phys. Rev. C **71**, 051602(R) (2005).

[2] L. A. Bernstein *et al.*, in *Proceedings of the International Conference on Nuclear Data for Science and Technology (ND2004) Santa Fe, NM*. AIP Conf. Proc. No. 769, edited by R. C. Haight, M. B. Chadwick, T. Kawano, and P. Talou (AIP, New York, 2005), pp. 890–893 (2005).

[3] J. Escher and F. S. Dietrich, LLNL Tech. Rep. no. UCRL-TR-212509-Draft, 2005 (unpublished).

[4] J. Escher and F. S. Dietrich, in *Second Argonne/MSU/JINA/INT RIA Workshop: Reaction Mechanisms for Rare Isotope Beams (Michigan State University, East Lansing, March 9–12, 2005)*, AIP Conf. Proc. No. 791, edited by A. Brown (AIP, New York, 2005), p. 93.

[5] J. Escher *et al.*, Nucl. Phys. **A758** 86c (2005).

[6] J. Escher *et al.*, J. Phys. G **31**, S1687 (2005).

[7] C. Forssén *et al.*, Nucl. Phys. **A758** 130c (2005).

[8] J. A. Church *et al.*, Nucl. Phys. **A758** 126c (2005).

[9] W. Younes and H. C. Britt, Phys. Rev. C **67**, 024610 (2003).

[10] W. Younes and H. C. Britt, Phys. Rev. C **68**, 034610 (2003).

[11] W. Younes, H. C. Britt, J. A. Becker, and J. B. Wilhelmy, LLNL Tech. Rep. No. UCRL-ID-154194, 2003 (unpublished).

[12] J. D. Cramer and H. C. Britt, Phys. Rev. C **2**, 2350 (1970).

[13] J. D. Cramer and H. C. Britt, Nucl. Sci. Eng. **41**, 177 (1970).

[14] H. C. Britt and J. B. Wilhelmy, Nucl. Sci. Eng. **72**, 222 (1979).

[15] F. S. Dietrich, LLNL Tech. Rep. No. UCRL-TR-201718, 2004 (unpublished).

[16] E. Gadioli and P. E. Hodgson, *Pre-Equilibrium Nuclear Reactions* (Clarendon Press, Oxford, 1992).

[17] J. T. Harke and L. W. Phair (private communication), 2005.

[18] R. Vandenbosch and J. R. Huizenga, *Nuclear Fission* (Academic Press, New York, 1973).

[19] Young, Chadwick, Talou, and Leal, ENDF/BVII β0 evaluation, MAT # 9228, Mar. 2005.

[20] W. Younes and H. C. Britt, LLNL Tech. Rep. No. UCRL-TR-212600, 2005 (unpublished).